A new GUV-based assay to reconstitute membrane tethering *in vitro* demonstrates the vesicle tethering ability of the selective autophagy scaffold Atg11.

Devika Andhare and Michael J Ragusa

Department of Chemistry, Dartmouth College, Hanover, NH 03755, USA

* Correspondence: michael.J.ragusa@dartmouth.edu

ABSTRACT

Membrane tethering is essential for the generation of organelle contact sites and to anchor incoming vesicles to their target membranes before vesicle fusion. During autophagy in yeast, tethering of 30 nm vesicles to cargo is one of the first steps in the generation of the isolation membrane that engulfs the cargo to be degraded. While membrane tethering is critical for cellular function, many of the current biochemical techniques to assay for membrane tethering rely on indirect readouts and are limited in their ability to monitor protein localization at sites of tethering. As such, we developed a fluorescence-microscopy-based GUV liposome tethering assay (GLT) to directly visualize membrane tethering and monitor protein localization at tethering sites simultaneously. We initially used GLT with engineered membrane tethers to demonstrate the ease of use,

versatility and sensitivity of the assay. We also demonstrated that the selective autophagy scaffolding protein Atg11 can bind, and tether negatively charged membranes but is unable to bind GUVs mimicking the charge of the outer mitochondrial membrane. Atg11 instead requires the selective autophagy receptor Atg32 to be recruited to mitochondrial membranes. Lastly, we demonstrate that Atg11 bound to Atg32 on GUVs can tether negatively charged vesicles to GUVs. Collectively, our results reconstitute one of the first steps during the initiation of mitochondrial autophagy and highlight the versatility of GLT to study a range of membrane tethering events biochemically.

29 # INTRODUCTION

30 Over the last two decades, an increasing number of studies have highlighted the
31 importance of membrane tethering events in cells[1]. Membrane tethering occurs when
32 individual proteins or multiprotein complexes bridge two different membranes holding
33 them within a defined distance, frequently less than 100 nm. These tethering events can
34 be homotypic, where both membrane compositions are identical, or more commonly
35 heterotypic, where two distinct membranes such as the plasma membrane and the
36 endoplasmic reticulum (ER) are tethered[2]. The main functions of membrane tethering in
37 cells are to generate organelle contact sites and to recruit vesicles to their target
38 organelles prior to fusion[3,4].

39

40 Due to the diversity of membrane tethering events in cells, the proteins required for
41 tethering vary dramatically in their size, domain architecture and mechanism by which
42 they tether membranes. One of the most direct membrane tethers is the extended
43 synaptotagmin (E-synt) family of proteins which functions to tether the plasma membrane
44 (PM) to the ER[5]. E-synt proteins interact directly with both the ER and PM allowing for a
45 single protein to generate an organelle contact site[6]. However, most organelle contact
46 sites require at least two proteins[2]. In these cases, the contact site is mediated by
47 separate proteins that are either integral membrane proteins, soluble proteins anchored
48 to the membrane by posttranslational modifications (PTMs), or peripheral membrane
49 binding proteins[1]. In some contact sites, additional proteins are required to bridge the
50 proteins that interact with membranes.

51 In vesicle fusion, large multisubunit tethering complexes, like the HOPS and CORVET
52 complexes, bind to RAB GTPases, that are anchored to the membranes by PTMs, and
53 SNARE proteins, embedded in membranes, to facilitate tethering[4,7,8]. These multisubunit
54 tethering complexes are soluble protein complexes that do not bind membranes directly
55 and instead require RABs and SNAREs for their recruitment to membranes[9]. Coiled-coil
56 tethers are another important family of proteins required for vesicle fusion in cells[10]. These
57 tethers contain long coiled-coil domains that bind to membrane-anchored RAB GTPases
58 on one side and either RAB GTPases or membrane directly on the other.

59

60 In addition to vesicle trafficking and contact site generation, membrane tethering also
61 plays a role in organizing vesicles for the catabolic process of autophagy. During
62 autophagy, cytosolic material, including organelles, are captured in double-membrane
63 vesicles, termed autophagosomes, and targeted to lysosomes to facilitate their
64 degradation[11]. As a part of this process, an autophagosomal membrane sheet is built
65 around the outside of the cargo to be degraded. Membrane tethering plays a role at
66 several stages in autophagy. In organelle autophagy, selective autophagy receptors
67 (SARs) embedded in organelle membranes recruit the autophagy initiation machinery to
68 the organelle to be degraded[12]. This results in tethering between the cargo membrane
69 and autophagosomal membrane which requires the selective autophagy scaffolding
70 protein, Atg11 in yeast or FIP200 in mammals[13-15]. After initiation, the SAR interacts with
71 a family of ubiquitin-like proteins, Atg8 in yeast and LC3 family members in mammals,
72 which are conjugated to phosphatidylethanolamine (PE) in the autophagosomal
73 membrane[16]. This interaction maintains tethering between the cargo and

74 autophagosomal membrane independent of Atg11 or FIP200[17]. In addition, we recently
75 demonstrated that the dimeric peripheral membrane binding protein Atg23 can tether
76 small autophagy precursor vesicles and that these tethering events play a role in
77 membrane recruitment during autophagy initiation[18].

78

79 Given the diversity of tethering events and proteins that facilitate these events, studying
80 membrane tethering has been challenging. This is particularly true in cells due to the
81 complexity of contact sites, the transient nature of tethering in vesicular trafficking and the
82 indirect nature of the available assays[19]. Fluorescently labeled proteins and bimolecular
83 fluorescence complementation have been used to determine if specific proteins or protein
84 complexes are located at potential tethering sites[19,20]. However, it's unclear if these
85 proteins are actively participating in tethering or if they are localized to these sites for
86 other purposes. Disrupting potential tethers in cells may not lead to a loss in the contact
87 site due to redundancy in tethers at the site[21]. In addition, a loss of contact sites or fusion
88 events in response to protein depletion or knockout could be due to indirect effects and
89 not necessarily due to direct loss in tethering ability. Therefore, biochemical approaches
90 have been critical to investigate if a protein or a protein complex is capable of mediating
91 membrane tethering. For example, biochemical studies have demonstrated the
92 importance of RABs and SNAREs for HOPS-mediated homotypic tethering events[22,23].
93 While these assays have been essential to shed light on the mechanisms of membrane
94 tethering, many commonly used biochemical assays rely on indirect measures of
95 tethering. This includes light scattering, turbidity assays and microscopy of liposome

96 clustering, which all monitor the increasing size of vesicle clusters as they are tethered
97 rather than two differentially labeled membranes being held together[24].

98

99 To investigate membrane tethering in vitro, we aimed to create an assay capable of
100 reconstituting and examining the diverse spectrum of membrane tethering events that
101 occur in cells. This encompasses both homotypic and heterotypic tethering events.
102 Additionally, we sought to establish an assay providing a more direct readout, enabling
103 independent monitoring of two distinct membranes while simultaneously tracking protein
104 recruitment to these membranes. Our objective was also to design an assay where one
105 of the membranes could be immobilized, facilitating real-time manipulation of tethering
106 events and allowing for the determination of tethering kinetics. This led to the
107 development of the GUV and Liposome Tethering (GLT) assay, building upon a method
108 recently employed in the study of membrane tethering by the autophagy protein Atg23[18].
109 We anticipate that GLT will find broad applicability in the biochemical investigation of
110 membrane tethering events.

111

112 # RESULTS

113 ## Fluorescence-microscopy-based GLT assay

114 To establish an assay to study membrane tethering *in vitro* we added extruded liposomes
115 to giant unilamellar vesicles (GUVs) labeled with different fluorophores in the presence of
116 a tethering protein (Figure 1). We reasoned that the large size of GUVs (typically 1 to 100

117 μm in diameter) would allow us to directly visualize liposomes tethered on the GUV
118 surface, thus eliminating ambiguities arising due to aggregation of liposomes and/or
119 protein. Moreover, GUVs would allow us to observe if a fluorescently tagged protein also
120 localizes at tethering sites. To initially demonstrate the feasibility of this assay we
121 engineered an artificial membrane tether by fusing the monomeric phosphatidylinositol-
122 3-phosphate(PI3P)-binding EEA1 $FYVE_{1337-1411}$ with GST (GST-FYVE)[25]. Since GST
123 dimerizes, this generates a stable dimer of EEA1 $FYVE_{1337-1411}$ with two PI3P binding sites
124 in a single protein complex. Similarly engineered tethers generated by linking membrane
125 binding domains to GST have been shown to facilitate tethering[26]. GUVs containing PI3P
126 were first incubated with GST-FYVE, followed by incubation with 400nm liposomes
127 containing an identical lipid composition to the GUVs except for a different fluorophore for
128 detection. GUVs mixed with PI3P-liposomes alone or with the addition of purified GST
129 showed no co-localization between GUVs and liposomes (Figure 2A and B). In contrast,
130 addition of PI3P-liposomes to GUVs pre-incubated with 1μM GST-FYVE showed robust
131 recruitment of liposomes to GUVs as illustrated by fluorescence intensity traces along the
132 surface of a GUV in the liposome fluorescence channel (Figure 2C). This demonstrates
133 that GST-FYVE mediates homotypic tethering. Comparison of liposome fluorescence per
134 micron calculated along the surface of GUVs further shows that tethering of liposomes to
135 GUVs only occurred in the presence of GST-FYVE thereby validating GLT for the study
136 of homotypic membrane tethering (Figure 2D). To determine if protein localization could
137 be observed at tethering sites, we inserted a GFP tag between the GST and FYVE
138 domains in our construct generating GST-GFP-FYVE. Repeating the assay with GST-
139 GFP-FYVE, we observed that the protein coats GUVs and tethers liposomes (Figure 2E).

140 In addition, fluorescence intensity traces revealed that areas with tethered liposomes
141 showed increased intensity of GST-GFP-FYVE demonstrating that protein is localized to
142 tethering sites highlighting the applicability of this technique to monitor protein
143 colocalization with tethering events *in vitro* (Figure 2F).

144

145 The sensitivity of GLT is comparable to commonly used tethering 146 assays

147 Having demonstrated that GLT can be used to monitor homotypic membrane tethering
148 we next sought to compare the sensitivity of this assay with some commonly used
149 techniques to measure membrane tethering. In most membrane tethering assays
150 liposomes are mixed with protein tethers which results in the clustering of vesicles. The
151 resulting increase in the size of liposome clusters, as measured by dynamic light
152 scattering (DLS), or an increase in the fluorescence intensity of liposomes as monitored
153 by microscopy have been frequently used to assay for membrane tethering[27-29].
154 Therefore, we compared tethering at increasing concentrations of GST-FYVE using DLS
155 and fluorescence microscopy-based liposome clustering with GLT. Extruded 400nm-
156 liposomes containing PI3P were mixed with GST-FYVE at concentrations ranging from
157 0.5μM to 4μM. Fluorescence microscopy (Figure 3A and B) and DLS (Figure 3C) revealed
158 that larger clusters of liposomes could be observed with the addition of 0.5μM of GST-
159 FYVE. These clusters grew progressively larger in response to increasing GST-FYVE
160 concentration and didn't show a significant increase in size beyond 2μM GST-FYVE
161 (Figure 3A and B). Similarly, GLT showed the recruitment of liposomes to GUVs with the

162 addition of 0.5μM of GST-FYVE and showed increasing tethering with increasing protein
163 concentration (Figure 3D and E). While all of these techniques demonstrated tethering,
164 non-significant differences in the amount of tethering were observed for all of the
165 techniques over some concentration ranges. This indicates that while these techniques
166 all demonstrate that membrane tethering occurred and was concentration-dependent,
167 they have differential sensitivity across small changes in protein concentration. These
168 results demonstrate that the sensitivity of GLT to detect tethering is comparable with DLS
169 and fluorescence microscopy-based methods to measure membrane tethering.

170

171 GLT can distinguish between membrane binding and tethering

172 One challenge in studying membrane tethering is differentiating between membrane
173 binding and tethering. This often requires two assays, one to examine membrane binding
174 and a second to monitor membrane tethering. However, we reasoned that GLT could
175 distinguish between these two possibilities in a single experiment which would make it a
176 powerful tool to combine with mutagenesis studies aimed to disrupt membrane binding or
177 tethering. To test this, we purified GFP-EEA1 $FYVE_{1337-1411}$ which lacks the dimerizing
178 GST and is therefore a monomer that should not be able to tether membranes. However,
179 without the dimerizing GST tag this protein showed minimal membrane binding and was
180 therefore not useful to distinguish between membrane binding and tethering
181 (Supplemental Figure 1). This result is consistent with previous studies that showed the
182 monomeric construct (amino acids 1337-1411) of EEA1 FYVE has a very low affinity for
183 PI3P[25]. Instead, we used the monomeric pleckstrin homology (PH) domain of

184 phospholipase C-delta 1 (PLC-delta) which has a high affinity for $PI(4,5)P_2$[30]. We purified
185 GFP-tagged PH domain with (GST-GFP-PH) and without (GFP-PH) the dimerizing GST
186 tag and tested their abilities to tether membranes using GLT. Both constructs of the PH
187 domain bound GUVs containing $PI(4,5)P_2$, although GST-GFP-PH showed higher binding
188 than GFP-PH which is consistent with an increased avidity for the membrane due to the
189 dimerization of the two PH domains (Figure 4A). Liposomes were recruited to GUVs in
190 the presence of the dimeric GST-GFP-PH demonstrating that this construct can efficiently
191 tether membranes. Fluorescence intensity traces along GUVs showed the peaks in
192 liposome fluorescence (cyan) were coincident with peaks in GST-GFP-PH fluorescence
193 further validating the use of GLT to monitor the presence of protein at membrane tethering
194 events (Figure 4B). If GFP-PH is capable of tethering liposomes to GUVs, albeit with less
195 efficiency due to the reduced membrane binding of GFP-PH, then normalizing the
196 integrated liposome fluorescence intensity to the GFP fluorescence intensity should give
197 similar ratios between both GST-GFP-PH and GFP-PH. However, GST-GFP-PH had
198 significantly higher liposome-to-protein fluorescence ratios as compared to GFP-PH
199 (Figure 4D). We therefore concluded that while GFP-PH retains membrane binding it is
200 incapable of tethering membranes. As such, GLT can be used to distinguish between
201 membrane binding and tethering by proteins using a single assay.

202

203 GLT demonstrates heterotypic tethering by the selective autophagy
204 Atg32-Atg11 complex

205 Next, we turned our attention to adapting GLT to reconstitute heterotypic tethering, which
206 involves protein-mediated bridging of membranes with distinct lipid compositions. For this,
207 we focused on tethering events that occur during mitochondrial selective autophagy,
208 termed mitophagy. Mitophagy begins with the selective autophagy receptor (SAR) Atg32,
209 embedded in the outer mitochondrial membrane, binding to the soluble scaffolding protein
210 Atg11[31,32]. Atg11 in turn recruits 30 nm precursor vesicles to mitochondria through its
211 interaction with the integral membrane protein Atg9 residing in these vesicles[13,33]. The
212 mammalian homolog of Atg11, FIP200, has been reported to bind membranes directly
213 once it binds to a SAR[15]. Based on this, we hypothesized that the binding of Atg32 to
214 Atg11 could initiate membrane binding by Atg11. If so, this suggests that we may be able
215 to reconstitute heterotypic membrane tethering by Atg32-Atg11 complex. To begin we
216 tested to see if Atg11 alone could bind, and tether vesicles made from yeast polar lipids
217 (YPL). To our surprise, GLT demonstrated that Atg11 alone was not only capable of
218 binding to YPL GUVs but it also was able to tether YPL GUVs and liposomes (Figure 5).
219 This demonstrates that Atg11 can bind membranes containing a high percentage of
220 negatively charged lipids (~42%) and suggests that Atg11 may serve as a homotypic
221 tether for autophagic precursor vesicles in cells through its interaction with both Atg9 and
222 membranes.

223

224 We next asked if Atg11 could be recruited to GUVs containing a lipid composition with a
225 similar charge (~20% negative charged lipids) to the outer mitochondrial membrane
226 (OMM) that are displaying the cytosolic domain of Atg32[34]. For this we fused the cytosolic
227 domain of Atg32(1-381), which binds to Atg11, with an N-terminal GFP and a C-terminal

228 10xHistidine tag (Supplemental Figure 2A). GUVs included 5 mol% of DGSNi^{2+}NTA to
229 allow for the recruitment of GFP-Atg32$_{1-381}$ to GUVs. To monitor Atg11 we labeled it with
230 Alexa Flour 594. GFP-Atg32$_{1-381}$ bound to GUVs containing DGSNi^{2+}NTA was able to
231 recruit Atg11. In contrast, Atg11 was not recruited to GUVs in the absence of Atg32
232 demonstrating that while Atg11 can bind YPL membranes it cannot bind GUVs containing
233 a similar charge to the OMM and instead requires Atg32 for its recruitment to autophagic
234 cargos (Supplemental Figure 2B).

235

236 To test if the Atg32-Atg11 complex could tether heterotypic membranes, we added
237 extruded YPL liposomes to GFP-Atg32$_{1-381}$ bound GUVs in the presence and absence of
238 Atg11 (Figure 6). YPL liposomes were tethered on GUVs only in the presence of Atg11
239 and the tethered liposomes colocalized with regions of higher Atg32 fluorescence (Figure
240 6C-E). These results demonstrate the ability of GLT to reconstitute and directly visualize
241 heterotypic tethering while also monitoring protein localization at these sites. From a
242 biological standpoint, while Atg9 is required for tethering *in vivo* this assay suggests that
243 mitochondrial-recruited Atg11 may also participate in these tethering events by binding
244 membranes directly to further enhance their recruitment and/or stabilize these tethering
245 events. Moreover, these results underscore the dual nature of some autophagy proteins,
246 wherein they are recruited to the cargo membrane through an interaction with SARs and
247 simultaneously engage the isolation membrane due to the presence of a high
248 concentration of negatively charged lipids in the autophagosomal membrane.

249

250 **GLT allows real-time visualization and kinetic analysis of membrane**
251 **tethering**

252 To test if GLT can be used to monitor membrane tethering in real-time, we attempted to
253 follow Atg11-mediated tethering of YPL liposomes on GFP-Atg32$_{1-381}$ bound GUVs. We
254 found that after 10 minutes of addition, GUVs settled and were non-specifically adhered
255 to LabTek chamber wells. We added GFP-Atg32$_{1-381}$ bound GUVs mixed with Atg11 on
256 LabTek wells and allowed them to settle. Next, we started acquiring a time-lapse imaging
257 sequence; added YPL liposomes and continued to monitor the fluorescence channel for
258 the liposomes (Supplemental Movie 1 and 2). On GUVs displaying GFP-Atg32$_{1-381}$ with
259 Atg11, liposomes started tethering on the GUV surface at 20 seconds after the liposomes
260 appeared in the background (Figure 7A). Liposomes remained bound to GUVs and
261 liposome fluorescence on GUVs increased over time. In contrast, on GUVs displaying
262 GFP-Atg32$_{1-381}$ alone, liposomes did not bind GUVs and could be seen diffusing around
263 GUVs throughout the length of the movie (Figure 7B). Analysis of the build-up of liposome
264 fluorescence on a line drawn along the GUV confirmed that liposome fluorescence
265 increased only in the presence of Atg11 (Figure 7C). The increase in liposome
266 fluorescence in the presence of Atg11 fit to a plateau followed by a one-phase exponential
267 rise equation and showed a t_{half} of 155 seconds, suggesting that tethering occurred in a
268 physiologically relevant timescale.

269

270 **DISCUSSION**

271 We demonstrated the broad usefulness of GLT to study membrane tethering *in vitro*. This
272 assay can be easily applied to study homotypic or heterotypic tethering events making it
273 ideal to reconstitute and examine tethering occurring at organelle contact sites and within
274 vesicle trafficking. We have shown that GLT has some significant advantages over
275 standard techniques for monitoring membrane tethering. First, it can be used to monitor
276 the localization of protein components at sites of tethering through three-color imaging.
277 Second, GLT can be used to distinguish membrane binding from tethering. In this way,
278 mutations made to individual proteins can be tested using GLT to determine if the
279 mutations lead to a loss of membrane binding, tethering or both. Lastly, GLT can be used
280 to monitor membrane tethering in real-time and the kinetics of membrane tethering can
281 be determined. We hope that real-time GLT can be employed in the future to monitor not
282 only tethering but also detethering providing new tools to study the regulation and
283 dynamics of tethering events.

284

285 In all of our GLT assays RhPE and DiD were used to label GUVs and liposomes,
286 respectively. It's important to note that exchange of these fluorophores was never
287 observed when membranes were tethered. This suggests that even though the
288 membranes are tethered in close proximity they are not brought close enough to trigger
289 fusion of the two membranes which would allow for the exchange of the fluorophores.
290 This suggests that GLT could be further adapted to monitor the exchange of the
291 fluorophores due to fusion events making it an even more powerful technique to study
292 membrane tethering.

293

294 To monitor tethering events, GLT quantifies the localization of liposomes on the surface
295 of GUVs. Consequently, GLT is limited in its ability to investigate tethering when both
296 membranes exhibit high curvature. GUVs are ideal for mimicking relatively flat membrane
297 surfaces in cells such as the PM, ER and mitochondria; while liposomes can be extruded
298 to mimic the curvature of vesicles, such as COP-II or clathrin-coated vesicles which are
299 between 40 and 100 nm in diameter[35,36].This makes GLT optimal for reconstituting
300 heterotypic tethering events where small vesicles are tethered to flat membranes prior to
301 vesicle fusion. For example, GLT may be a useful assay to reconstitute exocyst-mediated
302 heterotypic tethering of secretory vesicles to the PM[37].

303

304 Our work for the first time demonstrates that Atg11 can directly interact with and tether
305 membranes made from YPL. This result is in contrast to previous studies which
306 demonstrated that Atg11 was unable to bind membranes[13]. However, two key differences
307 could account for the observed variations in the biochemical abilities of Atg11. First, we
308 recombinantly expressed and purified Atg11 from HEK cell culture where it is a stable
309 dimer as opposed to recombinant expression and purification from *E. coli* where Atg11
310 behaves as a monomer. Second, we used YPL membranes that contain approximately
311 42% negatively charged lipids. In contrast, Atg11 was previously shown to not bind
312 liposomes composed of 60% POPC, 20% Cholesterol, 10% POPE and 10% POPS which
313 contain only 10% negatively charged lipids[13]. Therefore, it seems possible that Atg11
314 membrane binding requires a high negative charge which is consistent with the
315 composition of the autophagosomal membrane that contains 37% phosphatidylinositol
316 and low concentrations of phosphatidylserine and phosphatidic acid[38]. Atg11 membrane

317 binding may play important roles early in selective autophagy initiation. It may help in the
318 recruitment of Atg9 vesicles to selective autophagy initiation sites or it could help stabilize
319 tethering between cargo and autophagosomal membranes. In previous studies, we have
320 demonstrated that several autophagy proteins, including Atg13, bind to liposomes made
321 from YPL but not to membranes with a low concentration of negatively charged lipids[18,39].
322 This observation may suggest a common characteristic among several autophagy
323 proteins, wherein these proteins bind to the highly charged autophagosomal membrane
324 but are unable to bind to the less charged membrane of organelle cargos.

325

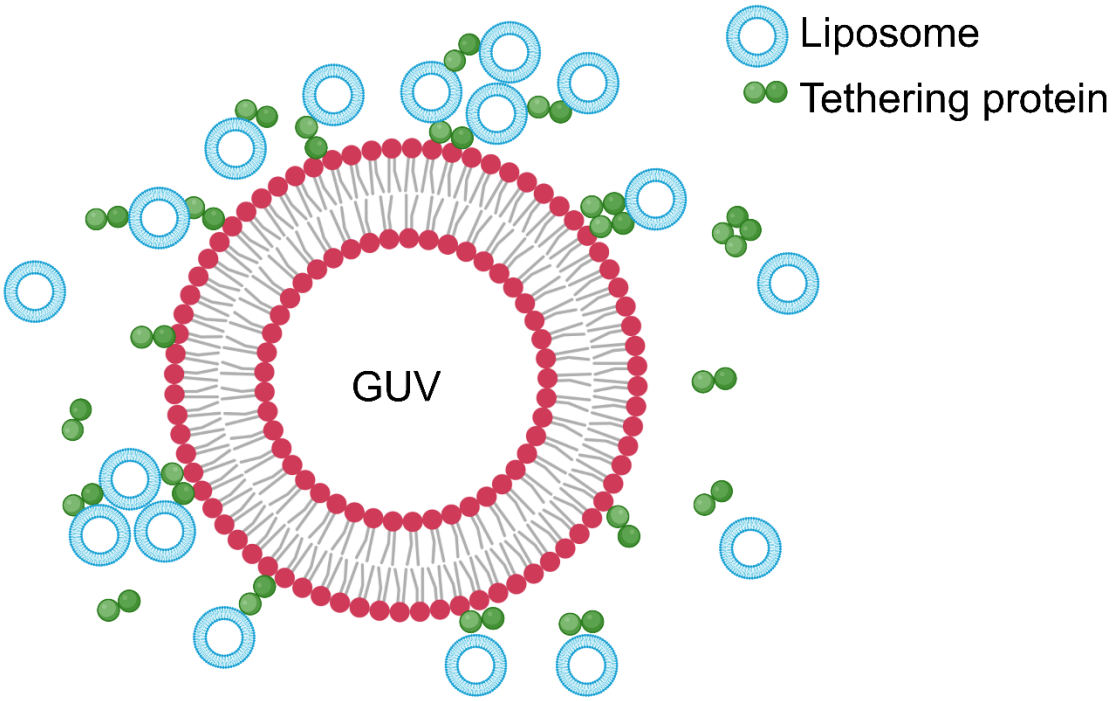

FIGURE 1. Schematic showing the fluorescence microscopy-based GLT assay. GUVs and liposomes containing different fluorophores are mixed with a candidate tethering protein or proteins capable of binding and bridging both membranes. Tethering is visualized by the co-localization of liposomes on GUVs in the presence of the protein.

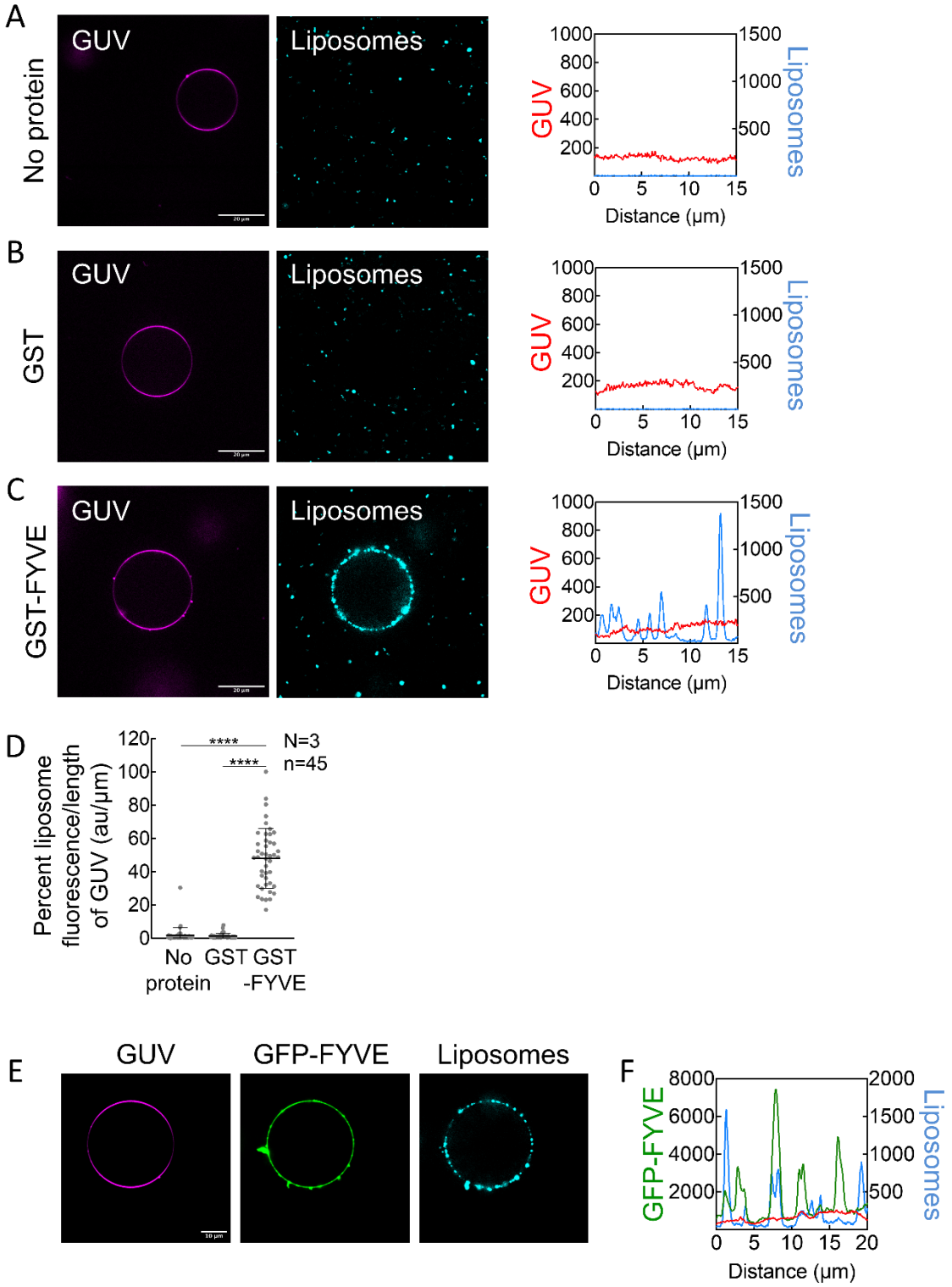

FIGURE 2. GLT using an engineered tether. 400 nm-extruded liposomes containing 74.9 mol% DOPC, 20 mol% DOPS, 5 mol% PI3P and 0.1 mol% of the fluorescent lipophilic dye DiD were incubated with GUVs containing 74.9 mol% DOPC, 20 mol% DOPS, 5 mol% PI3P and 0.1 mol% rhodamine PE (RhPE) in the presence or absence of different proteins. Representative images for liposomes mixed with GUVs (A), GUVs and

339 GST (B), or GUVs and GST-FYVE (C) are shown. Fluorescence intensity profiles for the
340 GUV and liposome channels along the circumference of the GUV are shown to the right
341 of each representative image. D) Scatter plots showing the percent of liposome
342 fluorescence per length of GUV normalized to the largest signal from A to C. Data from 3
343 independent repeats (N=3) were pooled and analyzed using non-parametric Mann-
344 Whitney's test. **** indicates $p<0.0001$. n indicates total number of GUVs analyzed for
345 each condition. E) GUVs containing PI3P were mixed with GST-GFP-FYVE followed by
346 incubation with PI3P-containing liposomes. Representative fluorescence images are
347 shown. F) Fluorescence intensity profiles for the GUV, liposome and protein fluorescence
348 channels around the circumference of the GUV shown in E.

349

350

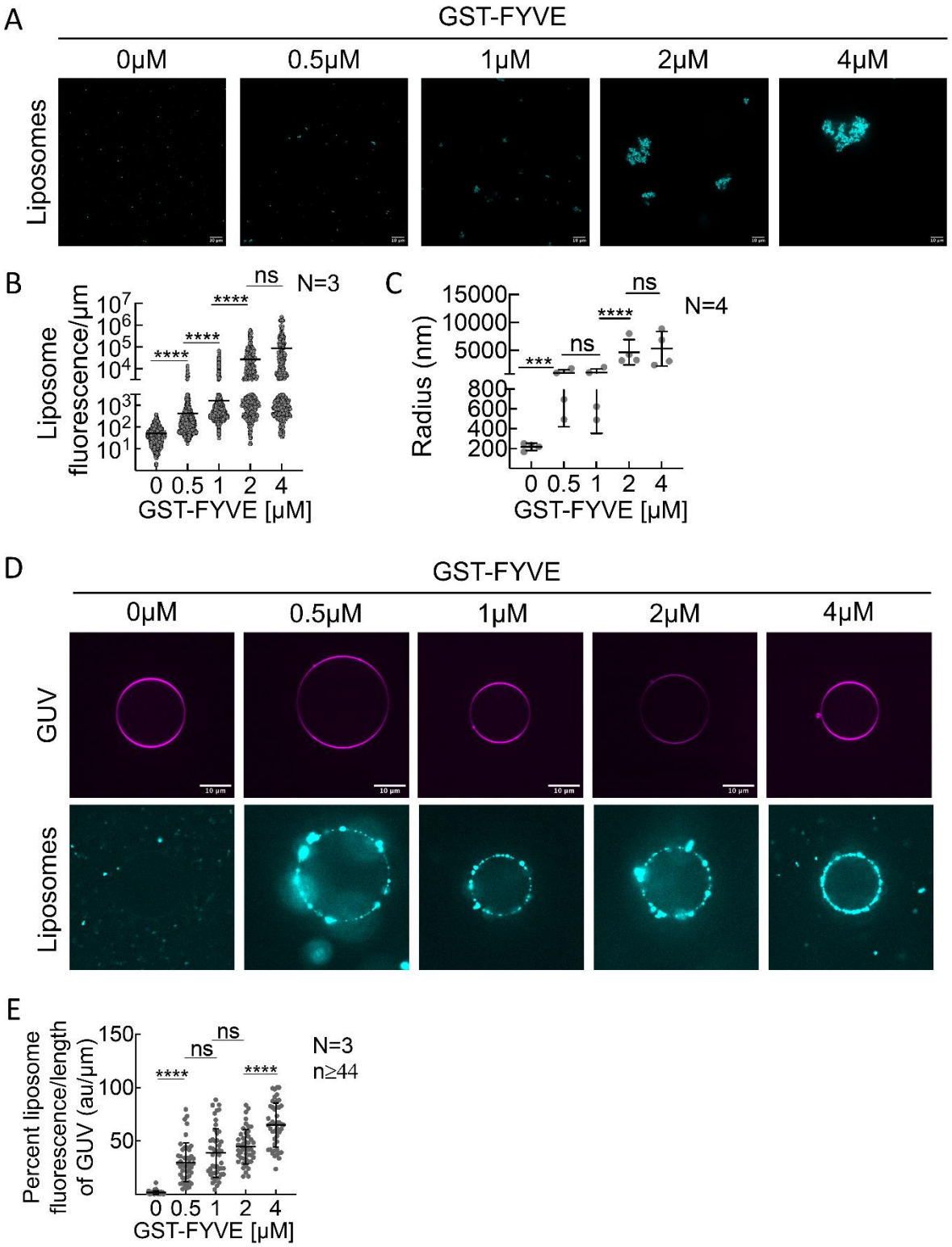

FIGURE 3. Comparison of GLT with two commonly used methods to study tethering. 400nm-extruded liposomes containing 74.9 mol% DOPC, 20 mol% DOPS, 5 mol% PI3P and 0.1 mol% of the fluorescent lipophilic dye DiD were incubated with increasing concentrations of GST-FYVE. Tethering was measured using fluorescence

356 microscopy (A and B) or DLS (C). A) Representative fluorescence images showing
357 clustering of PI3P-liposomes with increasing concentration of GST-FYVE. Scale
358 bar=10μm B) Quantitation of A. Data from 3 independent repeats (N=3) were pooled and
359 analyzed using Mann-Whitney's test. C) Quantitation of the increase in PI3P-liposome
360 size in response to increasing GST-FYVE concentration as measured by DLS. Data from
361 4 independent repeats (N=4) were analyzed using Mann-Whitney's test. ** indicates
362 p=0.0025, *** indicates p=0.0006. D) Representative fluorescence images from GLT
363 using liposomes as in A and GUVs containing 74.9 mol% DOPC, 20 mol% DOPS, 5 mol%
364 PI3P and 0.1 mol% RhPE in response to the addition of GST-FYVE at increasing
365 concentration. E) Quantitation of D. Data from 3 independent repeats (N=3) were pooled
366 and analyzed using Mann-Whitney's test. *** indicates p<0.0001. n indicates the total
367 number of GUVs analyzed per condition.

368

369

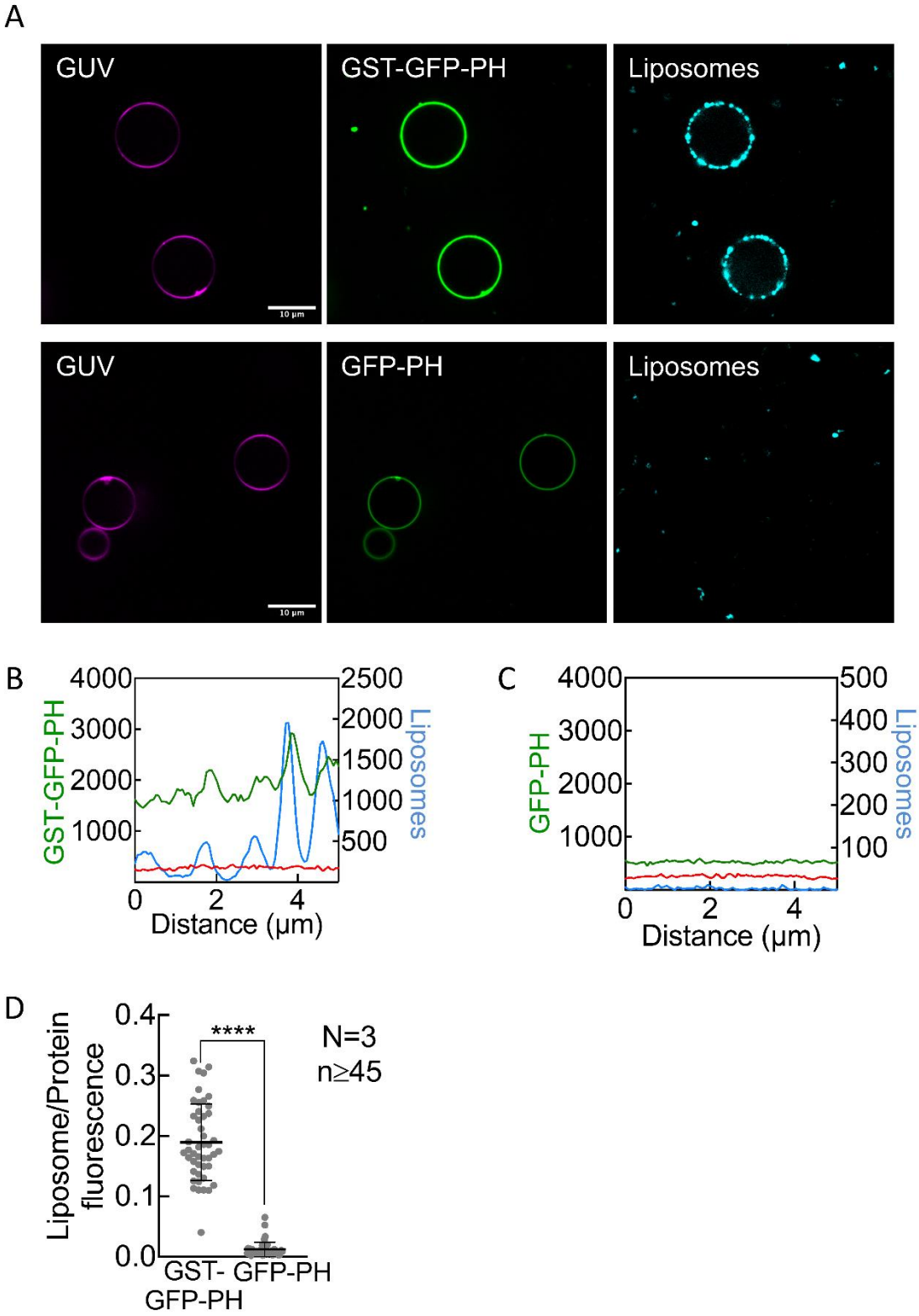

FIGURE 4: GLT of dimeric and monomeric PH domains with PI(4,5)P_2 membranes. GUVs containing PI(4,5)P_2 (magenta) were incubated with either GST-GFP-PH or GFP-

PH and subsequently mixed with PI(4,5)P_2-containing liposomes (cyan). A) Representative fluorescence images of GLT where GUVs were mixed with liposomes and either GST-GFP-PH (top panel) or GFP-PH (bottom panel). B) Fluorescence intensity profiles from a line drawn along the GUV in A (top panel) showing liposome and GST-GFP-PH fluorescence along the length of the GUV. C) Fluorescence intensity profiles from a line drawn along the GUV in A (bottom panel) showing liposome and GFP-PH fluorescence along the length of the GUV. D) Quantitation of A showing mean liposome fluorescence intensity from a segmented line drawn along the GUV surface normalized to mean protein fluorescence intensity. Data from 3 independent repeats (N=3) were pooled and analyzed using non-parametric Mann-Whitney's test. **** indicates $p<0.0001$. n indicated total number of GUVs analyzed per condition. GUVs were made with DOPC (74.9mol%), DOPS(20mol%), DOPI(4,5)P_2(5mol%), and RhPE(0.1mol%). Liposomes were made with identical composition except RhPE which was replaced with DiD.

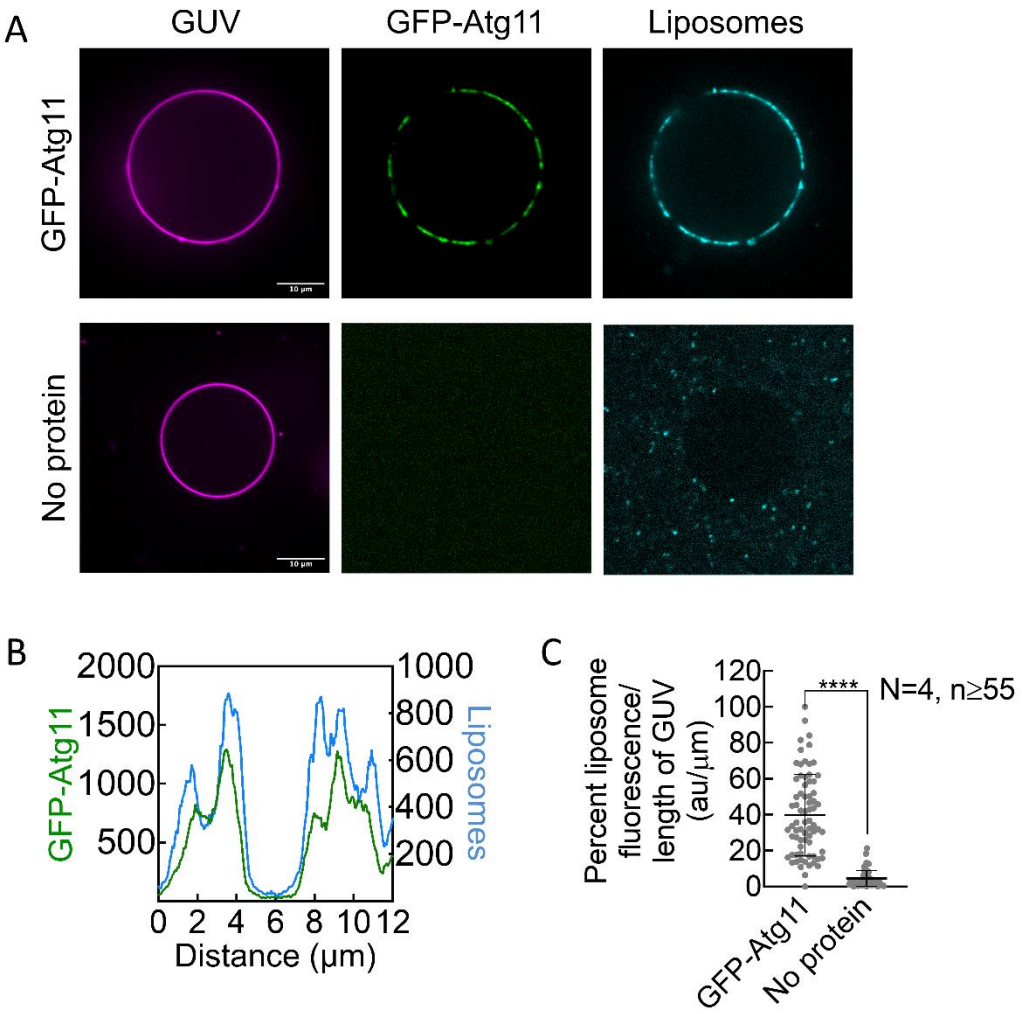

387

388 **Figure 5. GLT of Atg11 with GUVs and liposomes made from YPL.** GUVs (magenta)
389 made from YPL alone or premixed with GFP-Atg11 (green) were incubated with
390 liposomes (cyan) made from YPL. For visualization GUVs were made with 0.1% RhPE
391 and liposomes were made with 0.1% DiD. A) Representative fluorescence images with
392 GFP-Atg11 (top panel) and without any protein (bottom panel). B) Fluorescence intensity
393 profiles from a line drawn along the GUV in A (top panel). C) Quantitation of A showing
394 fluorescence intensity of liposomes normalized to the length of GUV in the presence and
395 absence of GFP-Atg11. n represents the number of GUVs analyzed. **** indicates
396 $p<0.0001$ analyzed using Mann-Whitney's test.
397

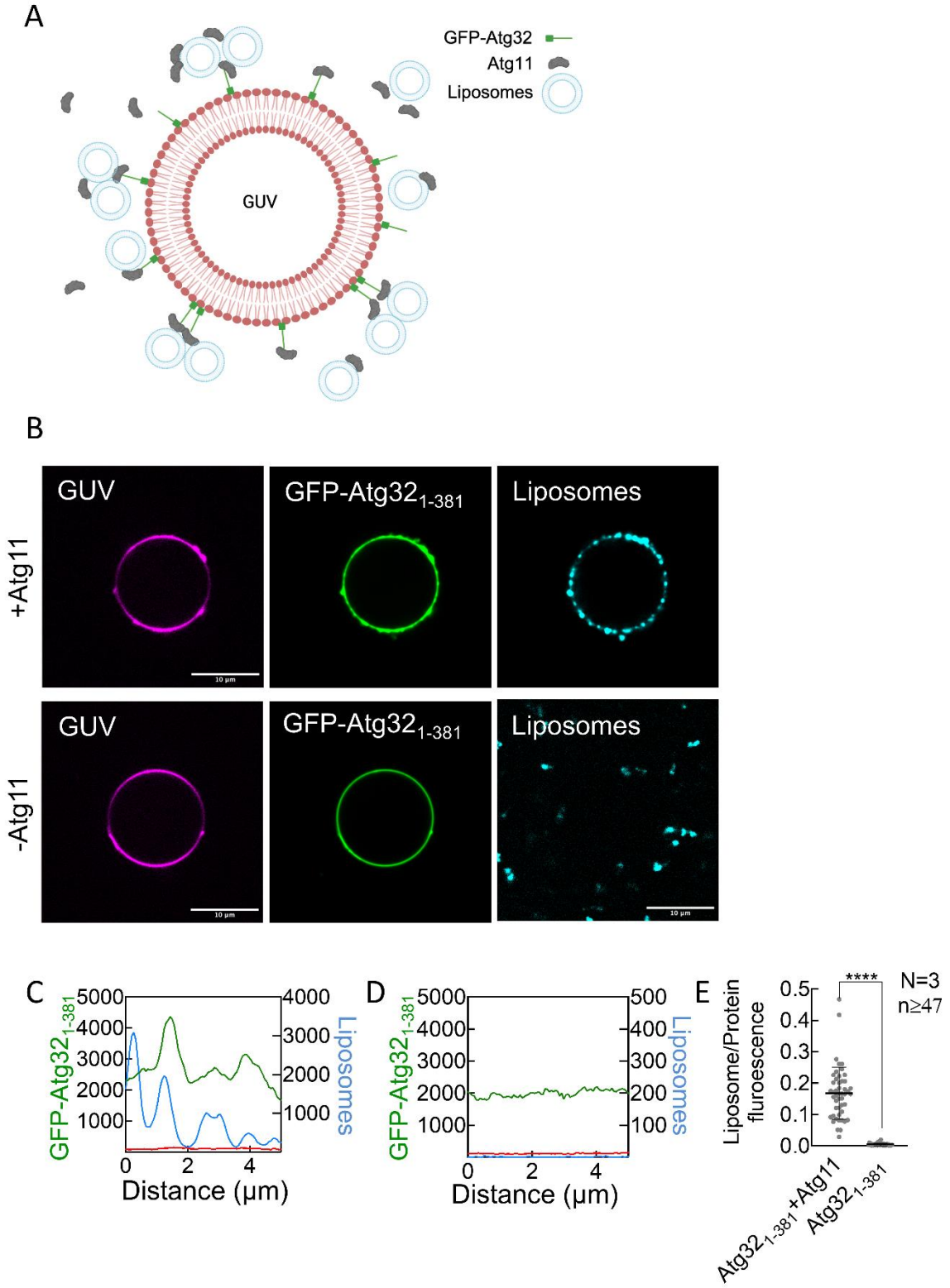

FIGURE 6. GLT testing the heterotypic tethering activity of the Atg32-Atg11 complex. A) Schematic showing heterotypic tethering reconstituted using GLT. B) Representative fluorescence images of GLT with GUVs (magenta) containing 5% mol DGS-Ni^{+2}NTA displaying His-GFP-Atg32$_{1-381}$ (green) which were sequentially incubated

403 with Atg11 and YPL liposomes (cyan) (top panel) or YPL liposomes (cyan) alone (bottom
404 panel). C) Fluorescence intensity profiles from a line drawn along the GUV in A (top panel)
405 showing liposome and GFP-Atg32$_{1-381}$ fluorescence intensities along the GUV. D)
406 Fluorescence intensity profiles from a line drawn along the GUV in A (bottom panel)
407 showing liposome and GFP-Atg32$_{1-381}$ fluorescence intensities along the GUV. E)
408 Quantification of the colocalization of liposomes and GFP-Atg32$_{1-381}$ fluorescence from
409 B. Data from 3 independent repeats (N=3) were pooled and analyzed using non-
410 parametric Mann-Whitney's test. **** indicates $p<0.0001$. n indicates the total number of
411 GUVs analyzed per condition. GUVs were made with DOPC (74.9mol%), DOPS
412 (20mol%), DGS-Ni^{+2}NTA (5mol%), and RhPE (0.1mol%). Liposomes were made with YPL
413 (99.9mol%) and DiD (0.1mol%).
414

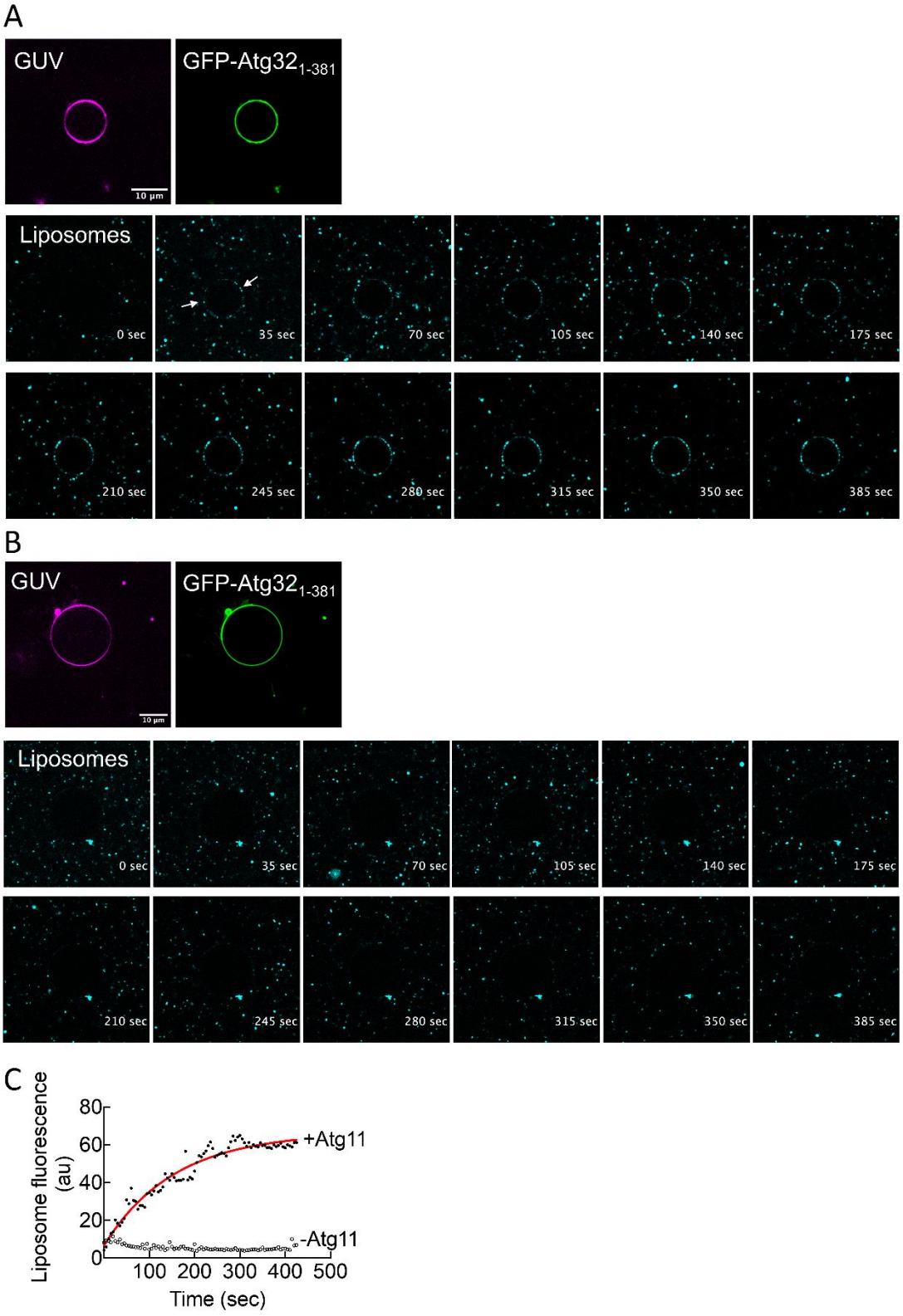

FIGURE 7. Real-time visualization and kinetic analysis of tethering using GLT. GUVs containing 5 mol% of DGS-Ni^{+2}NTA incubated with GFP-Atg32$_{1-381}$ and Atg11 or GFP-Atg32$_{1-381}$ alone were allowed to settle in a LabTek well. A time-lapse series was recorded

419 during the addition of YPL liposomes. A) A montage showing the real-time addition and
420 tethering of liposomes (cyan) to a GUV (magenta) bound to GFP-Atg32$_{1-381}$(green) and
421 Atg11. B) Montage showing the real-time addition of liposomes (cyan) to a GUV
422 (magenta) bound to GFP-Atg32$_{1-381}$(green). C) Representative trace showing the buildup
423 of liposome fluorescence on a line drawn along the GFP-Atg32$_{1-381}$ bound GUV surface
424 in the presence (filled circles) and absence (empty circles) of Atg11. The red line shows
425 the fit to a plateau followed by a one-phase exponential rise equation. GUVs were made
426 with DOPC (74.9mol%), DOPS(20mol%), DGS-Ni^{+2}NTA (5mol%), and RhPE(0.1mol%).
427 Liposomes were made with YPL (99.9mol%) and DiD (0.1mol%)
428

429

430 # MATERIALS AND METHODS

431 ## Recombinant protein expression and purification

432 All constructs used for protein purification in this paper are listed in Supplemental Table
433 1. The PH domain from GFP-C1-PLCdelta-PH was subcloned into pET His6 GST TEV
434 LIC cloning vector (1G) (Addgene plasmid # 29655 which was a gift from Scott Gradia)
435 to generate 12XHis-GST-GFP-PH. GFP-C1-PLCdelta-PH was a gift from Tobias Meyer
436 (Addgene plasmid # 21179)[40]. 6XHis-GST, 12XHis-GST-EEA1 FYVE, 12XHis-GST-GFP-
437 EEA1 FYVE, 12XHis-GST-GFP-PH and StrepII-GFP-Atg32(1-381)-10XHis were
438 recombinantly expressed in *E. coli* Star cells (Invitrogen C601003). Cultures were grown
439 in LB broth (Fisher Scientific, BP1426) to an OD_{600} of 0.6 to 0.8 at 37°C while shaking at
440 210 rpm. Cultures were cooled at 4°C for 20 min. Protein expression was induced by
441 adding 1 mM isopropylthio-β-D-galactopyranoside (IPTG; IBI Scientific, IB02125) and the
442 cultures were grown for an additional 18 h at 18°C. Cells were harvested and cell pellets
443 were stored at −80°C.

444 For purification of 6XHis-GST, 12XHis-GST-EEA1 FYVE, 12XHis-GST-GFP-EEA1 FYVE
445 and StrepII-GFP-Atg32(1-381)-10XHis, cell pellets were thawed and resuspended in
446 50 mM Tris pH 8, 500 mM NaCl, 2.5mM imidazole, 5mM $MgCl_2$, 1 mM
447 phenylmethanesulfonyl fluoride (PMSF; VWR, 0754) and cOmplete Mini EDTA-
448 free protease inhibitor tablets (Roche, 11836170001). Cells were lysed using 3 strokes of
449 a microfluidizer at 18000 psi. Triton X-100 (VWR, AAA16046-AE), was subsequently
450 added to lysates at 1% vol/vol. Lysates were spun at 25,000g for 30 minutes. The
451 supernatant was then applied to pre-equilibrated Talon resin (Clontech, 635504). The

452 resin was washed with 50 mM Tris, pH 8, 500 mM NaCl, 10 mM imidazole. Bound
453 proteins were eluted with 50mM Tris pH8, 500mM NaCl, 250mM imidazole. For
454 purification of 6XHis-GST, 12Xhis-GST-EEA1 FYVE, 12Xhis-GST-GFP-EEA1, peak
455 fractions containing protein were pooled and dialyzed against 20mM Tris pH 8, 300mM
456 NaCl and 0.2 mM TCEP. Proteins were aliquoted, flash-frozen in liquid nitrogen and
457 stored at −80°C. For purification of StrepII-GFP-Atg32(1-381)-10XHis, elutions from Talon
458 resin were pooled and incubated with pre-equilibrated Strep resin (IBA). The resin was
459 washed with 20 mM Tris pH8 and 300 mM NaCl. Protein was eluted with 20 mM Tris pH8,
460 300 mM NaCl and 50 mM biotin. Peak fractions containing protein were dialyzed against
461 20 mM Tris pH 8, 300 mM NaCl and 0.2 mM TCEP. Dialyzed protein was aliquoted, flash-
462 frozen in liquid nitrogen and stored at −80°C until use.

463 For purification of 12XHis-GST-GFP-PH constructs, cell pellets were resuspended and
464 thawed in 20 mM Tris pH 8.0, 500 mM NaCl, 2.5 mM imidazole, 1mM DTT and a cOmplete
465 Mini protease inhibitor tablet (Roche, 11836170001). Cells were lysed using 3 strokes of
466 a microfluidizer at 18000 psi. Triton X-100 (VWR, AAA16046-AE) was subsequently
467 added to lysates at 1% vol/vol. Lysates were spun at 25,000g for 30 minutes. Supernatant
468 was added to pre-equilibrated GST resin (add cat no) and incubated on a rocker for 1.5
469 hr at 4°C. Resin was washed with 20 mM Tris pH 8.0, 500 mM NaCl. The GST resin was
470 divided into two parts, one part was used for elution of GST-GFP-PH using 20 mM Tris
471 pH 8.0, 300 mM NaCl and 40 mM reduced glutathione. Eluted protein was dialyzed
472 against 20mM Tris pH 8.0, 300mM NaCl and 0.2mM TCEP. The other half of the GST
473 resin was incubated with TEV overnight at 4°C. Flowthrough from the GST resin
474 containing GFP-PH was subsequently incubated with Talon resin to remove TEV.

475 Flowthrough from the Talon resin was subjected to size exclusion chromatography using
476 a Superdex75 column. Peak fractions containing proteins were aliquoted, flash frozen in
477 liquid nitrogen and stored at −80°C until use.

478 Atg11 and GFP-Atg11, both with an N-terminal 2XStrep II tag, were recombinantly
479 expressed in Freestyle cells for 3 days post transfection. Cells were harvested by spinning
480 by 1000g for 15 mins. Cell pellets were flash frozen in liquid nitrogen and stored at −80°C.
481 Cell pellets were resuspended and thawed in 50mM Tris pH 8.0, 500mM NaCl, 1mM DTT,
482 1mM PMSF and a cOmplete Mini protease inhibitor tablet (Roche, 11836170001). Cells
483 were lysed using 3 strokes of a microfluidizer at 18000 psi. Triton X-100 (VWR,
484 AAA16046-AE), was subsequently added to lysates at 1% vol/vol. Lysates were spun at
485 25,000g for 30 minutes. Supernatant was applied to Strep resin (IBA) at 1mL/min using
486 a peristaltic pump. Resin was washed with 20mM Tris pH 8, 300 mM NaCl and 1 mM
487 DTT. Bound protein was eluted with 20mM Tris pH 8.0, 300mM NaCl, 50mM biotin and
488 1mM DTT. Fractions containing protein were pooled and concentrated to 2μM and flash-
489 frozen in liquid nitrogen. For GFP-Atg32 binding experiments, Atg11 was fluorescently
490 labeled with a three-fold molar excess of Alexa fluor 594 for 1hr at room temperature.
491 Labelling was quenched using 1 mM DTT. Unreacted dye was removed by dialyzing the
492 labelled protein against 20 mM Tris pH 8.0, 300 mM NaCl, 0.2 mM TCEP and 1 mM DTT
493 for 48 hrs. Fresh buffer was added after 24 hrs of dialysis.

494

495 **Liposome preparation**

496 All lipids were purchased from Avanti Polar lipids. Chloroform stocks of lipid mixtures at a
497 desired ratio containing 0.1mol% of the fluorescent lipophilic dye DiD were aliquoted in a
498 clean glass tube and dried under a gentle nitrogen stream until all the chloroform had
499 evaporated. Residual chloroform was removed under vacuum for 18 hrs. Dried lipids were
500 resuspended in 20 mM Tris pH 8, 150 mM NaCl to a final concentration of 1 mM. For
501 experiments with Atg11, YPL liposomes were resuspended in 20 mM Tris pH 8, 100 mM
502 NaCl to a final concentration on 1 mM. Liposomes were extruded using an Avanti Mini
503 Extruder using 0.4µm Nuclepore Track-Etched membrane (Sigma Aldrich,
504 WHA10417104).

505

506 **Giant unilamellar vesicle preparation**

507 GUVs were made using the gel-assisted formation method[41]. Briefly, chloroform stocks
508 containing lipids mixed at desired ratios containing the fluorescent lipid RhPE were
509 aliquoted in a glass tube. Chloroform was dried under a stream of nitrogen followed by
510 drying under vacuum (1 hr). The dried lipids were resuspended in fresh chloroform to
511 make a 1 mM lipid mixture. Polyvinyl alcohol (PVA, Mw = 14500; Sigma, 814894) was
512 dissolved in boiling water to make a 5% stock and degassed in a vacuum chamber. PVA
513 solution (10 µL) was spread into a thin film on a glass coverslip kept on a heating block
514 set to 55°C. Chloroform-dissolved lipid mix (10 µL) was then spread on the dried PVA
515 film. The dried PVA-lipid films were peeled from the glass coverslips and transferred to a
516 1.5-mL microcentrifuge tube. Films were hydrated in 300 µL assay buffer (20 mM Tris, pH

517 7.4, 100 mM NaCl) for 20 mins, and GUVs were released by gentle tapping. The PVA
518 films were removed using a pipette.

519

520 GUV liposome tethering (GLT)

521 For GLT experiments, GUVs were first mixed with tethering protein or control protein in a
522 1.5 mL Eppendorf tube for 10 min at room temperature. GUV mixtures were tapped to
523 resuspend settled GUVs and subsequently incubated with 10 µL of 400-nm extruded
524 liposomes for 5mins at room temperature. Liposomes were used within 3 days of
525 extrusion. The GLT mixtures (300µL total volume) were transferred to a BSA-passivated
526 LabTek chamber for imaging. GUVs were allowed to settle for 5 min prior to imaging.
527 LabTek chambers were treated with 3 M NaOH for 10 min followed by extensive washes
528 with milliQ water. NaOH-treated chambers were then passivated by incubation with BSA
529 (3mg/mL). BSA was removed by three washes with the assay buffer.

530 For real-time monitoring of GLT, GFP-Atg32$_{1-381}$ bound GUVs were incubated with Atg11.
531 GUVs displaying the GFP-Atg32$_{1-381}$-Atg11 complex were added to the BSA-passivated
532 LabTek chamber and allowed to settle for 5min. A field containing settled GUVs was
533 chosen, and real-time acquisition was started at 5 sec intervals. Liposomes (10 uL) were
534 added near the field under observation taking care not to disturb the settled GUVs.

535

536 Dynamic light scattering assay and microscopy-based liposomes
537 clustering assay

538 To monitor liposome tethering using DLS, GST-FYVE was spun at 100,000g for 20 min
539 to remove large aggregates. 50μL of PI3P-containing 400nm extruded liposomes were
540 mixed with increasing concentrations of GST-FYVE in a total volume of 80uL. The
541 liposome and GST-FYVE mixture was placed on a rocker and incubated for 30 minutes
542 at room temperature. Liposome size was measured using DynaPro NanoStar.

543 To measure liposome clustering, PI3P-containing liposomes (with 0.1 mol% of DiD) mixed
544 with GST-FYVE prepared as described above were added to a BSA-passivated LabTek
545 chamber. Liposomes were allowed to settle for 5 mins and ten fields were randomly
546 imaged for each GST-FYVE concentration.

547

548 **Fluorescence microscopy**

549 GLT and liposome clustering were imaged using a Nikon TiE microscope fitted with a
550 Yokogawa CSU-W1 spinning disk system using a 100 X, 1.45 NA oil immersion objective.
551 Images were acquired with a Photometrics Prime BSI sCMOS camera using the NIS
552 elements software.

553

554 **Image analysis**

555 Fluorescence microscopy images were analyzed using Fiji[42]. and statistical analysis was
556 performed using GraphPad Prism (version 5.0a).

557 All experiments were performed in at least triplicates. Data from three independent
558 repeats (N = 3) were pooled and plotted as scatterplots. Error bars represent standard
559 deviation.

560 Percent liposome fluorescence per length of GUV was calculated by normalizing the
561 liposome fluorescence, collected from a two-pixel wide segmented line drawn along a
562 GUV, to the length of the GUV. For calculating the liposome/protein fluorescence ratio,
563 fluorescence intensities in liposome and protein channels from a two-pixel wide
564 segmented line drawn along a GUV were collected. Mean liposome fluorescence was
565 divided by mean protein fluorescence to yield liposome/protein fluorescence ratios.

566 To analyze tethering using the microscopy-based liposome clustering assay, images were
567 first background corrected using the mode intensity value. Images were auto-thresholded.
568 Liposome fluorescence per micron was calculated using the integrated density values of
569 all particles with an area more than 0.2 μm^2.

570

571 **AUTHOR CONTRIBUTIONS**

572 D.A. and M.J.R. conceived and planned the experiments. D.A. carried out the
573 experiments. D.A. and M.J.R. drafted the manuscript.

574

575 **ACKNOWLEDGMENTS**

576 This work was supported by the National Institute of General Medical Sciences (NIGMS)
577 grant R35GM128663 to M.J.R. Expression of Atg11 was performed in the BioMT service

578 center and protein purification was performed in part performed at the BioMT Molecular
579 Tools Core which are both supported by NIGMS grant P20GM113132. Sequencing of
580 plasmids was performed by the Molecular Biology Shared Resource Center which is
581 supported by NCI Cancer Center Support Grant P30CA023108. We would also like to
582 thank Ann Lavanway for her work and support at the Dartmouth Imaging Facility.

583

584 **REFERENCES**

585

586 1. Szentgyörgyi V, Spang A. Membrane tethers at a glance. J Cell Sci 2023; 136.
587 doi:ARTN jcs260471
588 10.1242/jcs.260471.
589 2. Scorrano L, De Matteis MA, Emr S, Giordano F, Hajnoczky G, Kornmann B, et al.
590 Coming together to define membrane contact sites. Nat Commun 2019; 10:1287.
591 doi:10.1038/s41467-019-09253-3.
592 3. Phillips MJ, Voeltz GK. Structure and function of ER membrane contact sites with
593 other organelles. Nat Rev Mol Cell Biol 2016; 17:69-82. doi:10.1038/nrm.2015.8.
594 4. Ungermann C, Kümmel D. Structure of membrane tethers and their role in fusion.
595 Traffic 2019; 20:479-90. doi:10.1111/tra.12655.
596 5. Saheki Y, De Camilli P. The Extended-Synaptotagmins. Biochim Biophys Acta
597 Mol Cell Res 2017; 1864:1490-3. doi:10.1016/j.bbamcr.2017.03.013.
598 6. Bian X, Saheki Y, De Camilli P. Ca(2+) releases E-Syt1 autoinhibition to couple
599 ER-plasma membrane tethering with lipid transport. Embo J 2018; 37:219-34.
600 doi:10.15252/embj.201797359.
601 7. Spang A. Membrane Tethering Complexes in the Endosomal System. Front Cell
602 Dev Biol 2016; 4:35. doi:10.3389/fcell.2016.00035.
603 8. Jahn R, Scheller RH. SNAREs--engines for membrane fusion. Nat Rev Mol Cell
604 Biol 2006; 7:631-43. doi:10.1038/nrm2002.
605 9. Lurick A, Kummel D, Ungermann C. Multisubunit tethers in membrane fusion.
606 Curr Biol 2018; 28:R417-R20. doi:10.1016/j.cub.2017.12.012.
607 10. Cheung PY, Pfeffer SR. Transport Vesicle Tethering at the Trans Golgi Network:
608 Coiled Coil Proteins in Action. Front Cell Dev Biol 2016; 4:18.
609 doi:10.3389/fcell.2016.00018.
610 11. Parzych KR, Klionsky DJ. An overview of autophagy: morphology, mechanism,
611 and regulation. Antioxid Redox Signal 2014; 20:460-73. doi:10.1089/ars.2013.5371.
612 12. Vargas JNS, Hamasaki M, Kawabata T, Youle RJ, Yoshimori T. The mechanisms
613 and roles of selective autophagy in mammals. Nat Rev Mol Cell Biol 2023; 24:167-85.
614 doi:10.1038/s41580-022-00542-2.
615 13. Matscheko N, Mayrhofer P, Rao Y, Beier V, Wollert T. Atg11 tethers Atg9 vesicles
616 to initiate selective autophagy. PLoS Biol 2019; 17:e3000377.
617 doi:10.1371/journal.pbio.3000377.
618 14. Sawa-Makarska J, Baumann V, Coudevylle N, von Bülow S, Nogellova V, Abert
619 C, et al. Reconstitution of autophagosome nucleation defines Atg9 vesicles as seeds for
620 membrane formation. Science 2020; 369:1206-+. doi:ARTN eaaz7714
621 10.1126/science.aaz7714.
622 15. Shi X, Chang C, Yokom AL, Jensen LE, Hurley JH. The autophagy adaptor
623 NDP52 and the FIP200 coiled-coil allosterically activate ULK1 complex membrane
624 recruitment. Elife 2020; 9. doi:10.7554/eLife.59099.
625 16. Johansen T, Lamark T. Selective Autophagy: ATG8 Family Proteins, LIR Motifs
626 and Cargo Receptors. J Mol Biol 2020; 432:80-103. doi:10.1016/j.jmb.2019.07.016.
627 17. Kirkin V, Rogov VV. A Diversity of Selective Autophagy Receptors Determines the
628 Specificity of the Autophagy Pathway. Mol Cell 2019; 76:268-85.
629 doi:10.1016/j.molcel.2019.09.005.

630 18. Hawkins WD, Leary KA, Andhare D, Popelka H, Klionsky DJ, Ragusa MJ.
631 Dimerization-dependent membrane tethering by Atg23 is essential for yeast autophagy.
632 Cell Rep 2022; 39. doi:ARTN 110702
633 10.1016/j.celrep.2022.110702.
634 19. Huang X, Jiang C, Yu L, Yang A. Current and Emerging Approaches for Studying
635 Inter-Organelle Membrane Contact Sites. Front Cell Dev Biol 2020; 8:195.
636 doi:10.3389/fcell.2020.00195.
637 20. Jing J, Liu G, Huang Y, Zhou Y. A molecular toolbox for interrogation of
638 membrane contact sites. J Physiol 2020; 598:1725-39. doi:10.1113/JP277761.
639 21. Eisenberg-Bord M, Shai N, Schuldiner M, Bohnert M. A Tether is a Tether is a
640 Tether: Tethering at Membrane Contact Sites. Developmental Cell 2016; 39:395-409.
641 doi:10.1016/j.devcel.2016.10.022.
642 22. Shvarev D, Schoppe J, Konig C, Perz A, Fullbrunn N, Kiontke S, et al. Structure
643 of the HOPS tethering complex, a lysosomal membrane fusion machinery. Elife 2022;
644 11. doi:10.7554/eLife.80901.
645 23. Stroupe C, Hickey CM, Mima J, Burfeind AS, Wickner W. Minimal membrane
646 docking requirements revealed by reconstitution of Rab GTPase-dependent membrane
647 fusion from purified components. Proc Natl Acad Sci U S A 2009; 106:17626-33.
648 doi:10.1073/pnas.0903801106.
649 24. Ueda S, Tamura N, Mima J. Membrane Tethering Potency of Rab-Family Small
650 GTPases Is Defined by the C-Terminal Hypervariable Regions. Frontiers in Cell and
651 Developmental Biology 2020; 8. doi:ARTN 577342
652 10.3389/fcell.2020.577342.
653 25. Dumas JJ, Merithew E, Sudharshan E, Rajamani D, Hayes S, Lawe D, et al.
654 Multivalent endosome targeting by homodimeric EEA1. Mol Cell 2001; 8:947-58.
655 doi:10.1016/s1097-2765(01)00385-9.
656 26. Song H, Wickner W. Tethering guides fusion-competent trans-SNARE assembly.
657 Proc Natl Acad Sci U S A 2019; 116:13952-7. doi:10.1073/pnas.1907640116.
658 27. Ho R, Stroupe C. The HOPS/Class C Vps Complex Tethers High-Curvature
659 Membranes via a Direct Protein-Membrane Interaction. Traffic 2016; 17:1078-90.
660 doi:10.1111/tra.12421.
661 28. Nakatogawa H, Ichimura Y, Ohsumi Y. Atg8, a ubiquitin-like protein required for
662 autophagosome formation, mediates membrane tethering and hemifusion. Cell 2007;
663 130:165-78. doi:10.1016/j.cell.2007.05.021.
664 29. Segawa K, Tamura N, Mima J. Homotypic and heterotypic trans-assembly of
665 human Rab-family small GTPases in reconstituted membrane tethering. J Biol Chem
666 2019; 294:7722-39. doi:10.1074/jbc.RA119.007947.
667 30. Garcia P, Gupta R, Shah S, Morris AJ, Rudge SA, Scarlata S, et al. The
668 pleckstrin homology domain of phospholipase C-delta 1 binds with high affinity to
669 phosphatidylinositol 4,5-bisphosphate in bilayer membranes. Biochemistry 1995;
670 34:16228-34. doi:10.1021/bi00049a039.
671 31. Kanki T, Wang K, Cao Y, Baba M, Klionsky DJ. Atg32 Is a Mitochondrial Protein
672 that Confers Selectivity during Mitophagy. Developmental Cell 2009; 17:98-109.
673 doi:10.1016/j.devcel.2009.06.014.

32. Okamoto K, Kondo-Okamoto N, Ohsumi Y. Mitochondria-anchored receptor Atg32 mediates degradation of mitochondria via selective autophagy. Dev Cell 2009; 17:87-97. doi:10.1016/j.devcel.2009.06.013.
33. Coudevylle N, Banas B, Baumann V, Schuschnig M, Zawadzka-Kazimierczuk A, Kozminski W, et al. Mechanism of Atg9 recruitment by Atg11 in the cytoplasm-to-vacuole targeting pathway. J Biol Chem 2022; 298:101573. doi:10.1016/j.jbc.2022.101573.
34. Sperkagottlieb CDM, Hermetter A, Paltauf F, Daum G. Lipid Topology and Physical-Properties of the Outer Mitochondrial-Membrane of the Yeast, Saccharomyces-Cerevisiae. Biochim Biophys Acta 1988; 946:227-34. doi:Doi 10.1016/0005-2736(88)90397-5.
35. Miller EA, Schekman R. COPII - a flexible vesicle formation system. Curr Opin Cell Biol 2013; 25:420-7. doi:10.1016/j.ceb.2013.04.005.
36. Kirchhausen T, Owen D, Harrison SC. Molecular structure, function, and dynamics of clathrin-mediated membrane traffic. Cold Spring Harb Perspect Biol 2014; 6:a016725. doi:10.1101/cshperspect.a016725.
37. Lepore DM, Martinez-Nunez L, Munson M. Exposing the Elusive Exocyst Structure. Trends Biochem Sci 2018; 43:714-25. doi:10.1016/j.tibs.2018.06.012.
38. Schütter M, Giavalisco P, Brodesser S, Graef M. Local Fatty Acid Channeling into Phospholipid Synthesis Drives Phagophore Expansion during Autophagy. Cell 2020; 180:135-+. doi:10.1016/j.cell.2019.12.005.
39. Gatica D, Damasio A, Pascual C, Klionsky DJ, Ragusa MJ, Popelka H. The carboxy terminus of yeast Atg13 binds phospholipid membrane via motifs that overlap with the Vac8-interacting domain. Autophagy 2020; 16:1007-20. doi:10.1080/15548627.2019.1648117.
40. Stauffer TP, Ahn S, Meyer T. Receptor-induced transient reduction in plasma membrane PtdIns(4,5)P2 concentration monitored in living cells. Curr Biol 1998; 8:343-6. doi:10.1016/s0960-9822(98)70135-6.
41. Weinberger A, Tsai FC, Koenderink GH, Schmidt TF, Itri R, Meier W, et al. Gel-assisted formation of giant unilamellar vesicles. Biophys J 2013; 105:154-64. doi:10.1016/j.bpj.2013.05.024.
42. Schindelin J, Arganda-Carreras I, Frise E, Kaynig V, Longair M, Pietzsch T, et al. Fiji: an open-source platform for biological-image analysis. Nat Methods 2012; 9:676-82. doi:10.1038/nmeth.2019.